Department of Finance
Faculty of Business and Economics

Working Paper Series

Projecting Economic Loss with Climate Change

Jonathan Dark, Conrad Wasko, Julia Neme, Sarah Perkins-Kirkpatrick

Working Paper No. 01/25
August 2025

Projecting Economic Loss with Climate Change

Jonathan Dark[1], Conrad Wasko[2], Julia Neme[3], Sarah Perkins-Kirkpatrick[4]

[1]Department of Finance, University of Melbourne, Parkville, 3010, Australia
[2]School of Civil Engineering, The University of Sydney, Sydney, 2006, Australia
[3]Research School of Earth Sciences, Australian National University, Canberra 0200, Australia
[4]Fenner School of Environment and Society, Australian National University, Canberra 0200, Australia

Key Points:

- A flexible and robust methodology for projecting economic losses with climate change is presented
- Changes in the frequency and magnitude of flood events for Western North America are projected to the end of the century
- Economic losses associated with flooding for a high emissions scenario are projected to be double that of a low emissions scenario

Corresponding author: Jonathan Dark, jdark@unimelb.edu.au

Abstract

Climate change is increasing the magnitude and frequency of extreme weather events, leading to an increase in the economic losses from these natural disasters. Financial institutions, corporations, and governments are required to report on their exposures to climate change, in particular those related to meteorological hazards. Typically, approaches that project losses due to climate change employ top-down approaches using impact models and damage curves. Despite their high levels of complexity, the confidence in these approaches is low. We propose a novel approach to calculate future economic losses, using a physically based statistical approach that is directly linked to future climate projections. The approach is general and can be applied to any economic risk from extreme weather. We model aggregate loss distributions using a nonstationary multivariate Poisson distribution to model the frequency of events, and a conditional generalized Pareto distribution to model the magnitude of the events. These distributions employ demographic and climate covariates which are easily projected from climate model simulations. We illustrate our method by estimating the flood risk to property for Western North America. By the end of the century, the estimated economic losses under a high emissions scenario (SSP585) are twice the magnitude of the estimates under a rapid emissions reduction and negative emissions pathway (SSP126), highlighting the importance of meeting the Paris climate agreement targets.

1 Introduction

Extreme rainfall is projected to increase in magnitude and frequency (Myhre et al., 2019; Gründemann et al., 2022; Seneviratne et al., 2012) leading to increased flood risk (Trenberth et al., 2003; Westra et al., 2014). This is particularly the case for the most extreme events and in urban settings (Wasko & Nathan, 2019a; Fadhel et al., 2018; Hettiarachchi et al., 2018; Miller & Hutchins, 2017), thereby exacerbating the economic impacts of catastrophic flood events (Arent et al., 2014; IPCC, 2012). Dynamical and statistical downscaling project increased insurance losses due to anthropogenic climate change over the rest of this century (Held et al., 2013; Jevrejeva et al., 2018; Dottori et al., 2018). The economic cost of hurricane Harvey has already been attributed to anthropogenic climate change (Frame et al., 2020), with more historical studies finding increases rather than decreases in economic loss (Bouwer, 2011). Despite the overwhelming evidence for increased economic losses, there is a debate as to whether these increased economic losses are due to human influence on the global climate system (Neumayer & Barthel, 2011; Nicholls, 2011). This is in part due to (1) the complexity of the methodologies used for modelling changes in economic losses and (2) the complexity in modelling the impact of climate change on the catastrophe. For example, while increases in extreme rainfall lead to increased flooding, particularly in urban areas (Hettiarachchi et al., 2018), some floods have been shown to reduce with climate change. This is due to a complex change in antecedent conditions, and shifts from snow melt-driven to rainfall-driven flooding worldwide (Ivancic & Shaw, 2015; Sharma et al., 2018; Wasko, 2022; Zhang et al., 2022; Blöschl et al., 2019)

Approaches to modelling the impact of climate change on the economy can be broadly categorised as either (1) economic models termed Integrated Assessment Models (IAMs), which link climate covariates to GDP, or (2) Catastrophe (CAT) models which follow the chain of models approach, downscaling climate change impacts, modelling the changed hazard, and ultimately linking the change in hazard to the change in loss. Both model classes are complex and heavily parameterised. Goodess et al. (2003) reviewed many of the earlier IAMs which were fundamentally statistical and designed to be all encompassing, capturing the complex interactions (including feedback effects) between society and the environment. More recently Tol (2024) performed a meta-analysis on a wide range of more recent studies that increasingly rely on computable general equilibrium models or econometric analysis. Both reviews demonstrated that many studies only predicted

a mild impact from climate change on the global economy. Some studies even concluded the global economy or specific countries will be unaffected or benefit from climate change (Desmet & Rossi-Hansberg, 2015; Newell et al., 2021; Tol, 2002; Horowitz, 2009; Kahn et al., 2021). The meta-analysis of Tol (2024) for example showed that 2.5°C of warming would make the average person feel as though they had only lost 1.7% of their income. The uncertainty across models, means there must be more than 4°C of warming before there will be a negative impact that is statistically significant.

The findings of only a mild impact from climate change are in stark contrast to the dire warnings of the impacts of climate change from the scientific community (Rogers et al., 2025; Ho et al., 2025). IAMs may be unrealistic as they discount away the utility of future generations, thereby ignoring the serious impacts of climate change at the end of the century (Ackerman et al., 2009). Findings are also very sensitive to the shape of the damage function (Burke et al., 2018; Pezzey, 2019), and are likely to be unreliable when distributional outcomes have fat tails (Weitzman, 2009), which is often the case when modeling extreme (rare) events. One of the key issues is the use of historical data to fit econometric relationships that may not hold in a warmer future. Further, the models are typically calibrated to best fit central tendencies, not the tail of the distributions, which makes extrapolation to future rare events challenging.

Rather than focus on the mean, CAT models emphasise extreme events. This model class is generally utilised by insurers to quantify the risks of potential claims. These models typically contain (1) a module to generate potential events; (2) a hazard module that uses climate and geospatial data to estimate the intensity and location of each event; (3) an engineering module that has detailed data about the assets to quantify the damage; and (4) a financial module to calculate potential claims. CAT models typically employ highly granular geospatial data. Implementation requires considerable judgement, calibration and fine tuning. CAT modelling of future economic losses mimics the standard chain of models approach to impact modelling (Hakala et al., 2019). Here, a climate scenario is chosen, and this forms the boundary conditions for which the influence on the hazard (e.g. extreme rainfall or flooding) is modelled at the local scale, before the financial cost is calculated.

The high level of detail in CAT models suggests high levels of precision. However, even without considering the uncertainty due to climate change, CAT models often provide wildly different estimates due to their high level of parameterization (Cabantous & Dupont-Courtade, 2015). Weinkle and Pielke Jr (2017) for example report that a risk manager could with 95 percent confidence, select any value between $33-$192 billion USD as an estimate of hurricane risk in Florida. They therefore argue that CAT risk estimates are a function of choice, preferences and politics, rather than science. Although examples of flood risk impact modeling are abundant in the literature (Madsen et al., 2014; Fadhel et al., 2018; Hirabayashi et al., 2013; O'Shea, Nathan, Wasko, Ho, & Sharma, 2024; Alfieri et al., 2015), the proprietary nature of CAT models means that research on climate change and CAT models is sparse (Thistlethwaite et al., 2018).

Flood analysis using CAT modelling typically uses daily precipitation scenarios from downscaled Global Climate Models (GCMs) as inputs into a hydrological model to physically simulate flood peaks. An extreme value distribution is fit to the flood peaks, and results are translated into damages. This requires data on topography, asset distribution, population density and depth-damage functions (Alfieri et al., 2015; Arnell & Gosling, 2016; Bouwer et al., 2010). Given the complexities surrounding the causes of flooding, Ogden (2021) argues the hydrological models used in such impact analyses suffer from huge uncertainties, heterogeneities, non-linearities and other poorly understood phenomena - not withstanding the uncertainties in downscaling, and model and scenario choice (Hakala et al., 2019). Linking simulated flood peaks to damages is even more uncertain. Merz et al. (2010) and Jongman et al. (2012) critique the huge variety of damage models that differ substantially. For example Jongman et al. (2012) compare seven flood dam-

age functions across similar regions in Europe. At an inundation depth of 2 metres for example, the percentage damage to asset values varies from approximately 10% to 85%. Uncertainty in the depth damage curves and asset values is therefore far more important than uncertainties in the hydrological models. Despite this, damage functions are often "treated as some kind of appendix within the risk analysis" (Merz et al., 2010).

Due to the existential threat climate change poses, financial institutions, corporations and governments are now required to report and manage the long term tail risks associated with climate change (Fiedler et al., 2024) and hence projection of economic loss is now a mandatory requirement. International Financial Reporting Standards (IFRS S1 and S2) require disclosures about climate related risks over the short, medium and long term. However, the methods currently used to project economic losses are subject to low confidence. This is in part due to the high levels of discretion involved in the modeling process, as well as the sensitivity of results to assumed relationships and parameter values, with many of the parameters, relationships and inputs often uncertain.

To overcome the uncertainties in the projection of future economic losses, and address the need for institutions to model their future exposure to climate risks in a robust, parsimonious, and defensible manner, we present a novel approach to calculate future economic loss. We combine a non-stationary multivariate Poisson distribution to model the frequency of extreme events for each grid cell, with a conditional Generalised Pareto distribution (GPD) to model their severity. Our statistical distributions are linked to historical climate and demographic covariates. This allows projections of demographics and climate under Shared Socioeconomic Pathways (SSPs 126, 245, 370 and 585) (O'Neill et al., 2016) to simulate 10 year aggregate loss distributions from 2020-29 to 2080-89. Given that flooding is by far the most pervasive climate risk (McDermott, 2022), we illustrate our method by considering property damage from flooding across the IPCC Sixth Assessment Report (AR6) reference region of Western North America (WNA) (Iturbide et al., 2020). While previous literature has modeled changes in climatic extremes via extreme value distributions linked to covariates (Maposa et al., 2017; O'Shea, Nathan, Wasko, & Sharma, 2024; Osman et al., 2015; Khaliq & Cunnane, 1996), to our knowledge this presents the first attempt at modeling extreme losses directly using non-stationary extreme value analysis.

2 Methods

We seek to project an expected aggregate loss distribution for a geographic region (WNA) over a given time period. To do so, we combine a non-stationary multivariate Poisson distribution with conditional Generalised Pareto distributions. In Section 2.1 we discuss estimation of non-stationary univariate Poisson and conditional GPDs for each grid cell. In Section 2.2 we extend our methods to projection in the multivariate setting. We allow for spatial dependence between event occurrence across grid cells (via a non-stationary multivariate Poisson distribution). Consistent with the data, our severity distributions have tail event magnitudes that are cross-sectionally and inter-temporally independent.

2.1 Parameter estimation

Loss records are typically short in duration and irregularly spaced in time. We therefore employ a peak over threshold approach, by modeling both the arrival and intensity of the catastrophic event and its associated loss. Consider the economic loss as a random variable Z_i where $i = 1, ...N$ are the events above a threshold μ, and the number of events N occurring within a year is also a random variable. The frequency of the events is assumed to follow a Poisson distribution:

$$P\left(N=k\right)=\frac{e^{-\lambda(t)}\lambda(t)^{k}}{k!} \tag{1}$$

Where λ is the arrival rate of the extreme events which is allowed to vary with time t. The magnitude of the loss Z_i is modeled using a GPD, represented by:

$$F(y)=1-(1+\xi y)^{-1/\xi}\ \ \xi\neq 0 \tag{2}$$

$$F(y)=1-\exp(-y)\ \ \xi=0 \tag{3}$$

where ξ is the shape parameter, $y=(Z-\mu)/\sigma$, and $\sigma>0$ is the scale parameter. We allow the scale and shape parameter to vary as a function of covariates. As loss distributions are highly positively skewed, we impose $\xi>0$ and $\sigma>0$ by:

$$\sigma(X^{T}\alpha)=\exp(X^{T}\alpha) \tag{4}$$

$$\xi(X^{T}\beta)=\exp(X^{T}\beta) \tag{5}$$

where X denotes the matrix of covariates, and α and β denote parameter vectors.

To calculate the loss for a geographical region (here WNA) over a given time period, we divide the region into grid cells equivalent to each WNA state. GCMs have horizontal grids of varying sizes. For all climate metrics, we calculate values per state by doing a weighted average of the GCM grid cells pertaining to the state. The weights are calculated to represent the percentage of the state area that the grid cell occupies. So, for state i, the weight of cell j will be $W_j=A(i\cap j)/A_i$, where $A(i\cap J)$ is the area of the cell j contained within state i and A_i is the total area of the state, so $\sum_j W_j=1$.

The marginal λ for each state (or grid cell) is the total number of events divided by the number of years. To estimate the GPD parameters, we measure our losses on a real per capita basis for each state. We then use a maximum likelihood estimator to fit conditional GPDs to the pooled losses (across all WNA states), given temporal and spatial independence (see Section 3.2). The conditional scale and shape parameters are therefore the same across all states, but their projections vary for each state's climate model simulation. Given the complexities associated with flooding, we consider a wide range of covariates. To prevent overfitting of the GPDs we consider a maximum of two covariates for each model at a time. We consider all possible covariate combinations ranging from a model with no covariates, to one where either the scale or shape parameters have two covariates.

2.2 Projection of loss distributions

To project the aggregate loss distribution for a geographical region, the frequency and magnitude distributions are simulated for each cell (i.e each WNA state), and then aggregated. The frequency is projected using a simple linear trend in the rate parameter, while the magnitude distribution is projected from GCM realizations of the covariates.

Here an ensemble of ten GCMs are chosen for the covariate realizations (see Section 3.3), and we use the five best GPD models for each GCM based on the Akaike Information criterion (AIC). This means that to capture the projection uncertainty for a given SSP, 50 GPDs are considered for each replication when simulating aggregate loss distributions. For a given SSP (126, 245, 370, 585) the following steps are performed:

1. For a given year, simulate the number of extreme events for each grid cell. This is done via a random draw from the multivariate Poisson distribution. While the magnitude of the events is spatially independent, their occurrence is not, so spatial correlations are preserved between event occurrence using the NORTA correction (Yahav & Shmueli, 2012).
2. For each grid cell with non-zero tail events, the magnitude of the economic loss per capita is simulated via a random draw from a GPD with GCM simulated covariates. For the covariates that are normal by construction, we obtain a random draw beyond the 90th percentile from the gaussian density. For the remaining covariates, we obtain 240 months of covariate values (120 months backward looking, 120 months forward looking) and fit a stationary GPD to the top 10% of observations (24 data points). We note that the 20 year window is consistent with the IPCC assessment for assessing changes in temperature and precipitation extremes, and it can be assumed that precipitation extremes are appropriately stationary over this time window (Kharin et al., 2007).
3. The simulated loss is scaled by the population projection for the grid cell.
4. The simulated losses for each grid cell are aggregated to obtain region wide aggregated losses.
5. Steps 2-4 are repeated for the remaining GPDs associated with the first GCM. The simulated loss for the first GCM is the median estimate from GPDs 1 to 5. Steps 2-4 are then repeated for the remaining nine GCMs. This provides 10 aggregate losses for the year, one for each GCM.
6. This process is repeated for each year in the time horizon.
7. The Value at Risk (VaR) is calculated for the time horizon as the relevant percentile of the aggregate losses for that region - e.g. the 95% VaR is the 95th percentile of the simulated future losses.

Our loss simulation performs 1000 replications, which produces 10,000 aggregate losses for each year (1000 simulated losses for each of the 10 GCMs). For simulations over the 1960-2014 validation period, we calculate the mean, median, 90th and 95th percentiles for each GCM as well as across all GCMs. For our projections (from 2015-2089), we calculate the same metrics for temporally aggregated losses across decades (2020-29, 2030-39,..., 2080-89).

3 Data

The methodology is demonstrated by estimating property losses from flooding for the WNA region. The states within the WNA region are Arizona, California, Colorado, Idaho, Montana, New Mexico, Nevada, Oregon, Utah, Washington and Wyoming. Each geographical state represents one grid cell - hence we model a total of 11 grid cells (Figure 1). Finer resolution modeling could be attempted in the future, as loss data is available at the county level, but more granular modeling was not attempted here as (1) the GCM grid sizes used for covariate modeling are larger than most counties, and this would even apply to some of the regional climate models, and (2) county level loss data is unreliable, as losses are often equally distributed across affected counties within the state.

3.1 Property flood loss data

Loss data are provided by SHELDUS: a hazard data set maintained by Arizona State University Centre for Emergency management and Homeland security (ASU Center for Emergency Management and Homeland Security, 2025). It consists of direct property damage from flooding for each WNA state on a monthly basis from 1960. The loss for each state is converted to a per capita value using the population estimate as at 2020. As the historical CMIP6 simulations terminate at 2014, for consistency we use loss data

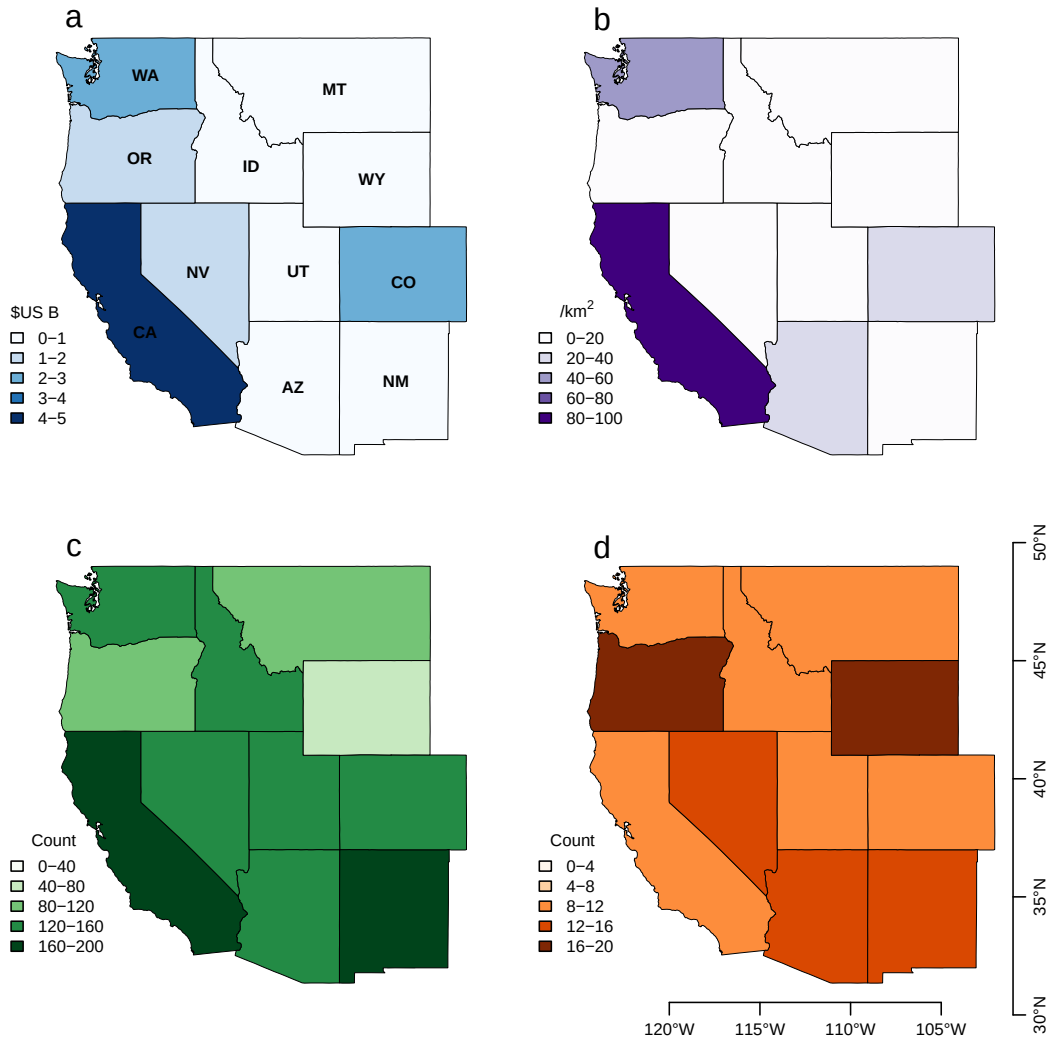

Figure 1. Property flood loss data per state. (a) Total losses in billion USD for each state (b) Population density (c) Total number of observed catastrophes (d) Number of observed catastrophes in the top 10%. Details are presented in Table 1.

up to and including 2014. Coastal flooding is excluded and WNA is not subject to hurricanes, so we avoid the complications associated with compound events.

Here only observations in the tail are used, defined as the top 10% of pooled per capita losses. Threshold selection involves a tradeoff between bias (where too many observations include non-tail events, violating the asymptotic theorem) and variance (where too few observations increase parameter uncertainty). Scarrott and MacDonald (2012) review the huge variety of methods used to determine the threshold ranging from graphical, rules of thumb, probabilistic and computational. Here we employ the upper 10% rule of thumb commonly applied in practice (DuMouchel, 1983; McNeil & Frey, 2000). Direct property losses from flooding totaled 13.94 billion USD (in 2020 dollars). The top 10% of flood events (146 obs) total 12.78 billion USD - 92% of total losses. Similar percentages apply to the losses in each decade. These results highlight the heavy right tail of the loss distribution, the need for extreme value analysis, and the reasonableness of the loss simulation assumption that observations below the threshold are zero.

Table 1 reports direct property losses from 1960-2014 by WNA state, with these losses and the population density summarized in Figure 1. Although the cost of flood events is highest in California, largely due to the higher population density, flood events both in total and in the tail are fairly evenly spread across all states. The tail events for each state also represent a high percentage of the total loss across all states. The exception is New Mexico where tail events only represent 64% of the total loss. The total population and population density are highly correlated with tail losses - with correlations of 0.88 and 0.92 respectively.

Table 1. Direct property losses from flooding by WNA state (1960-2014)

	All observations		Tail observations			Population 2020	
State	No obs	Loss $bn	No obs	Loss $bn	% tot loss	Tot M	Density (/km^2)
Arizona (AZ)	152	0.874	16	0.733	84%	7.2	24.3
California (CA)	186	4.603	12	4.048	88%	39.5	98.0
Colorado (CO)	136	2.116	11	2.041	96%	5.8	21.5
Idaho (ID)	129	0.237	9	0.206	87%	1.8	8.6
Montana (MT)	100	0.097	12	0.077	80%	1.1	2.9
New Mexico (NM)	178	0.232	14	0.148	64%	2.1	6.7
Nevada (NV)	123	1.181	15	1.142	97%	3.1	10.9
Oregon (OR)	97	1.604	17	1.563	97%	4.2	17.0
Utah (UT)	151	0.727	11	0.665	91%	3.3	15.4
Washington (WA)	126	2.119	10	2.014	95%	7.7	44.8
Wyoming (WY)	80	0.150	19	0.142	95%	0.6	2.3
Total	1458	13.940	146	12.778	92%	76.4	

The non-stationary GPD modeling requires independence between events (Beirlant & Goegebeur, 2003; Ma et al., 2020). Cross-sectional dependence is possible in per capita flood losses, as an extreme flood event may occur in several states. Inter-temporal dependence across months is less likely as most floods are short lived. To test for both forms of dependence, a panel from 1960 to 2014 by US state was created, where months without a flood loss in the tail are zero. The average correlation is 0.0389, with a median of -0.0040 and a 90th percentile of 0.1292. These low levels of cross sectional dependence are consistent with the CD test statistic of 1.4532 (p-value 0.15), which fails to reject the null of no cross-sectional dependence (Moscone & Tosetti, 2009). The panel Ljung Box test statistic of 41.605 (p-value 1.00) for a lag of 1, also fails to reject the null of no serial correlation. We conclude the per capita loss does not suffer from cross-sectional or inter-temporal dependence and estimate our GPDs using all the raw data.

3.2 Change rate for the Poisson Distribution

Despite clear increases in extreme rainfall (Sun et al., 2021), globally there is no clear evidence that flood frequency has increased over recent decades (Kundzewicz et al., 2014; Yang et al., 2021). Indeed, one is more likely to not find a climate change signal in flood data due to high variability in flood observations (Villarini & Wasko, 2021). However, the frequency of extreme precipitation is expected to increase throughout this century, and it's expected that flood frequency will increase as a result, particularly for the rarest events (Wasko et al., 2023). While further research is required into the appropriate climate covariates for non-stationary frequency models, as the dynamic drivers vary across regions (O'Shea, Nathan, Wasko, & Sharma, 2024), we accept that the frequency of flood events will change in the future. We don't link our Poisson parameter to covariates, as is performed for the GPD. Instead, we update λ each year from 2015 to 2089 based on linear estimates (Table 2) of projected changes in the probability of exceedance for extreme rainfall published in Li et al. (2021). While an approximation, we note that these rates of change correspond to other published observed and projected trends (Papalexiou & Montanari, 2019; Myhre et al., 2019). As Li et al. (2021) present their ratios/scaling

factors as a function of temperature increases relative to a 1985-2014 baseline, this increase in frequency is linearly apportioned over 2015 to 2089 by dividing by the temperature increase. Different scaling factors are applied for different SSPs to respect the non-linearity of the scenarios.

Table 2. λ scaling factors for multivariate Poisson distribution over projection period

SSP	Warming 2081-2100 rel to 1985-2014 (°C)	Scaling factor final year (2089)	Scaling factor increase per year
126	0.8	1.075	0.00100
245	1.7	1.203	0.00271
370	2.6	1.535	0.00714
585	3.4	1.852	0.01136

3.3 GPD Covariates

Given that floods are complex and generated by different processes, we consider a range of GCM covariates designed to capture precipitation intensity and duration, soil conditions, urbanisation and temperature. We consider the following covariates for each WNA state: 1) maximum 5 day precipitation (inches per day); 2) maximum 1 day precipitation (inches per day); 3) 3 month standardised precipitation; 4) 6 month standardised precipitation; 5) 12 month standardised precipitation; 6) total precipitation (inches per day); 7) population density (total state population/land size (km^2)) and 8) monthly average temperature.

Standardized precipitation indices are a transformation of the probability of a given amount of precipitation in "x" months. The index is zero at the median. The greater the departure from zero, the drier (-) or wetter (+) an event lasting "x" months compared to the long-term. This allows comparisons at different locations with very different climates; an index value at one location is the same relative departure from the median as another location. Indices are calculated at different time scales since it is possible to experience dry conditions at one time scale but wet conditions over another. The indices may be viewed as a proxy for the pre-existing soil conditions, noting that for more extreme rainfall events, soil conditions are less important (Wasko & Nathan, 2019a).

We evaluate CMIP6 models against observed rainfall from the Rainfall Estimates on a Grid Network (REGEN) (Contractor et al., 2020) for each index in Isphording et al. (2024). This resulted in the selection of ten CMIP6 GCMs (Table 3). For each GCM, we use the first member of the ensemble. As stated in section 2.1, the covariate for each state is a weighted average of the areas of the GCM grid cells that overlapped the state area.

While climate change has caused increasing losses from extreme weather, increases in population, wealth, and assets in at risk areas also increase losses (Bouwer et al., 2010; Changnon et al., 2000; Crompton & McAneney, 2008). Asset price inflation and wealth effects are controlled by using losses in current (2020) US dollars. Consistent with the per capita loss, the GPD fitting over 1960-2014 employs state level population densities as at 2020. For the projections (2015-2089), we use population density as a proxy for changes in urbanisation and assets at risk. While each SSP consists of a qualitative narrative and quantified projections for population, the SSPs have been developed on a global and national scale, and do not account for changes within a nation. The main population growth scenario from the US census bureau as at 2023 is therefore used, and it assumed the total percentage change applies to all states. For the years 2015-2023 we calculate population densities using actual population.

Table 3. CMIP6 models included in this study.

Model	Resolution	Institution	Reference
ACCESS-ESM1-5	250km	Commonwealth Scientific and Industrial Research Organisation, Australia	(Ziehn et al., 2020)
ACCESS-CM2	250km	Commonwealth Scientific and Industrial Research Organisation, Australia	(Bi et al., 2020)
BCC-CSM2-MR	100km	Beijing Climate Centre, China	(Wu et al., 2019)
CanESM5	500km	Canadian Centre for Climate Modelling and Analysis, Environment and Climate Change Canada, Canada	(Swart et al., 2019)
CMCC-ESM2	100km	Euro-Mediterranean Centre on Climate Change, Italy	(Lovato et al., 2022)
CMCC-CM2-SR5	250km	Euro-Mediterranean Centre on Climate Change, Italy	(Lovato et al., 2022)
MIROC6	250km	JAMSTEC (Japan Agency for Marine-Earth Science and Technology, Japan), AORI (Atmosphere and Ocean Research Institute, The University of Tokyo, Japan), NIES (National Institute for Environmental Studies, Japan), and R-CCS (RIKEN Centre for Computational Science, Japan)	(Tatebe et al., 2019)
MPI-ESM1-2-LR	250km	Max Planck Institute for Meteorology, Germany and Alfred Wegener Institute and Helmholtz Centre for Polar and Marine Research, Germany	(Mauritsen et al., 2019)
NorESM2-LM	250km	NorESM Climate modeling Consortium consisting of CICERO (Center for International Climate and Environmental Research), MET-Norway (Norwegian Meteorological Institute), NERSC (Nansen Environmental and Remote Sensing Center), NILU (Norwegian Institute for Air Research), UiB (University of Bergen), UiO (University of Oslo) and UNI (Uni Research), Norway	(Seland et al., 2020)
NorESM2-MM	100km	NorESM Climate modeling Consortium consisting of CICERO (Center for International Climate and Environmental Research), MET-Norway (Norwegian Meteorological Institute), NERSC (Nansen Environmental and Remote Sensing Center), NILU (Norwegian Institute for Air Research), UiB (University of Bergen), UiO (University of Oslo) and UNI (Uni Research), Norway	(Seland et al., 2020)

4 Results

The results are presented in three parts. First the estimation of the parameters is presented. The performance of the model is then evaluated by presenting estimates of the historical VaR. Finally, future loss estimates are projected using a positive linear trend in the arrival frequency of events and GCM covariates for event severity.

4.1 Parameter estimation

The marginal Poisson parameter for each state (λ) is estimated from the top 10% of losses per capita from the pooled data from 1960-2014. The marginal λ for each state is the total number of events divided by the number of years (55). The parameters are reported in Table 4. For example, Arizona expects 0.291 extreme flood events per year (2.91 per decade), similar to the other states.

In addition, our frequency distribution needs to preserve the correlation between tail events across the WNA states. The correlations in Table 4 are based on a panel that records the number of tail events by state per annum. So that a standard Cholesky decomposition can be employed, we use the NORTA (NORmal To Anything) correction (Yahav & Shmueli, 2012) when generating the number of tail events per year.

Table 4. Multivariate Poisson distribution parameters (annual frequency)

	Ariz	Calif	Color	Idaho	Mont	New Mex	Nevada	Oregon	Utah	Wash	Wyom
Marginal density											
λ	0.291	0.218	0.200	0.164	0.218	0.255	0.273	0.309	0.200	0.182	0.364
Extreme flood event correlations											
Ariz	1.000	0.038	-0.079	-0.042	0.042	0.193	0.035	-0.044	0.128	-0.061	0.071
Calif	0.038	1.000	0.237	0.485	0.427	-0.084	0.374	0.223	0.507	0.079	-0.093
Color	-0.079	0.237	1.000	0.416	0.064	0.193	0.534	0.386	0.262	0.098	-0.143
Idaho	-0.042	0.485	0.416	1.000	0.534	-0.114	0.395	0.383	0.612	0.141	-0.096
Mont	0.042	0.427	0.064	0.534	1.000	0.000	0.269	0.392	0.459	0.087	0.215
New Mex	0.193	-0.084	0.193	-0.114	0.000	1.000	-0.046	-0.016	-0.064	-0.044	0.069
Nevada	0.035	0.374	0.534	0.395	0.269	-0.046	1.000	0.414	0.269	0.227	-0.019
Oregon	-0.044	0.223	0.386	0.383	0.392	-0.016	0.414	1.000	0.318	0.068	-0.059
Utah	0.128	0.507	0.262	0.612	0.459	-0.064	0.269	0.318	1.000	0.003	0.005
Wash	-0.061	0.079	0.098	0.141	0.087	-0.044	0.227	0.068	0.003	1.000	0.033
Wyom	0.071	-0.093	-0.143	-0.096	0.215	0.069	-0.019	-0.059	0.005	0.033	1.000

Table 5 reports the top 5 GPD models and their selected covariates for each GCM. The last column for each model reports the AIC. To illustrate, the best model for GCM1 uses the first covariate (maximum 5 day precipitation) as a conditional scale parameter (α). The shape parameter (β) is estimated unconditionally. Standardised 3 month precipitation (Covariate 3) was never selected. Temperature (Covariate 8) was also never selected as we imposed a condition that the coefficients need to be strictly positive, and the correlation between the economic loss and temperature was always negative. The best models were more likely to have a non-stationary scale parameter (61 times) than shape parameter (15 times). Overall, population density and total precipitation were the most common covariates. The most frequently used scale covariates were population density (24 times), total precipitation (17 times), and 5 day maximum precipitation (13 times). Of the standardized precipitation metrics, the 12-month horizon was selected only once. For the shape parameter, the most frequently used covariates were total precipitation (5 times) and standardised 6 month precipitation (5 times).

Using a criteria of 1 AIC unit as a model improvement, 30 of the non-stationary models (out of the 50 models) provide a better fit than the stationary model. This would suggest retaining all GPDs from GCMs 1, 2, 4, 6, 8 and 9 and removing all GPDs from GCMs 3, 5, 7 and 10. While we could have removed these models, they are retained for completeness as their coefficient estimates are reasonable, and their inclusion in an ensemble can improve projection (Wang et al., 2023).

Table 5. Top 5 GPD models for each GCM. Covariate numbers listed in Section 3.3

	Model 1			Model 2			Model 3			Model 4			Model 5		
GCM	α	β	AIC	α	β	AIC	α	β	AIC	α	β	AIC	α	β	AIC
1	1		884.8	1,7		884.9	6,7		885.2	2,7		885.5	6		885.5
2	1,7		884.0	1		884.3	6,7		885.0	6		885.7	1	4	886.2
3	7		886.8	7	1	887.3	7	5	887.5			887.7	1,7		887.8
4	6		879.0	6,7		880.3	6	5	880.6	5,6		881.0	1,6		881.0
5	7		886.8	6,7		887.0	6		887.3	1,7		887.6	2,7		887.6
6	6		885.4	6,7		885.4	7	6	886.2		6	886.5	6	4	886.7
7	7		886.8	2,7		887.6			887.7	2		887.9	7	2	888.0
8	1		884.9	1,7		885.4	6,7		885.5	2		885.7	6		885.9
9	1	4	882.2	2	4	882.8	1		883.9	6	4	884.2	1	6	884.6
10	7		886.8			887.7	7	6	887.9		6	888.4	7	2	888.6

4.2 Historical Evaluation

To evaluate the fitted models, we simulate the yearly aggregate loss distribution over the sample period using the multivariate Poisson parameters in Table 4 and the 50 GPD models in Table 5. This is performed both with the observed historical data for each of the covariates, as well as the GCM simulated covariates. For the non-Gaussian covariates, we employ a +/- 10 year window to fit the stationary GPD to each covariate, and test our annual VaR estimates against aggregate WNA flood losses from 1960 to 2004. Consistent with the GPD calibration in Table 5, we use a constant population (and density) as at 2020 for each year. For comparison we also include VaR estimates using a stationary (i.e. no covariate) loss distribution, obtained by aggregating tail losses for all months in the year across the WNA states. The VaR estimate for a given level of confidence is the corresponding percentile.

If the loss simulations are well calibrated, observations that exceed the VaR should occur at a rate consistent with the confidence level. To illustrate, at a 95% level of confidence, actual flood losses should only exceed the VaR estimate 5% of the time. To formally test this we consider the test of Kupiec (1995). Let N = the number of times the loss exceeds the VaR estimate, T = the total number of observations, N/T = the VaR violation rate, and p = 1 - the level of confidence. The test has a null $H_0 : N/T = p$, an alternative $H_a : N/T \neq p$ and a critical value of χ^2_1.

Table 6 reports results for 90% and 95% VaR levels. All approaches fail to reject the null at conventional significance levels, suggesting our loss simulations are well calibrated. The simulations with covariates however, are no better than an estimate using no covariates. This is consistent with inconclusive evidence surrounding the impacts of climate change on historical flood risk (Kundzewicz et al., 2014). The same however cannot be said for the latter part of this century, as the impacts of climate change are expected to increase. Projections over the coming decades require time-varying densities, as unconditional estimates are likely to seriously underestimate tail risks.

Table 6. Historical simulation of VaR

VaR	Avg VaR ($bn, USD)	N	Rate (%)	Kupiec test statistic	p-value
Unconditional density					
90%	7.109	3	6.7	0.622	0.430
95%	9.708	2	4.4	0.030	0.862
Simulation using actual covariates					
90%	4.955	6	13.3	0.508	0.476
95%	7.914	3	6.7	0.239	0.625
Simulation using GCM covariates					
90%	6.521	5	11.1	0.060	0.807
95%	10.641	2	4.4	0.030	0.862

4.3 Projections

Aggregate losses are projected for SSP126, 245, 370 and 585. We employ the GPDs from Section 4.1, and the non-stationary multivariate Poisson distribution parameters which are scaled each year according to the ratios in Table 2. Table 4.3 reports the mean, median, VaR 90% and VaR 95% loss estimates by decade for each SSP. We omit GCM9 (BCC-CSM2-MR) estimates as they were 2-3 times greater than the remaining GCMs. For illustration, consider SSP245. The average loss across all WNA states for the 2020s in current dollars, is projected to be 4.621 billion USD. This will increase to 6.414 billion USD (current dollars) in the 2080s. The 95% VaR estimates suggest that 95% of the time, losses in the 2020s will not exceed 12.353 billion USD, but this threshold will in-

crease to 16.806 billion USD over the 2080s. Higher warming scenarios result in considerably higher loss estimates, with the VaR at the 95% level in the 2080s under SSP585 estimated at 28.028 billion USD. This is double the estimate under SSP126 of 14.323 billion USD.

Table 7. Direct property damage from flooding (current billions USD)

	2020s	2030s	2040s	2050s	2060s	2070s	2080s
SSP126							
mean	4.373	4.876	4.965	5.180	5.403	5.476	5.444
median	3.133	3.486	3.509	3.649	3.876	3.905	3.820
VaR 90%	8.499	9.345	9.494	9.821	10.242	10.642	10.330
VaR 95%	11.441	12.801	12.897	13.600	13.962	14.395	14.323
SSP245							
mean	4.621	4.708	5.213	5.455	5.638	5.999	6.414
median	3.337	3.396	3.832	4.041	4.106	4.315	4.610
VaR 90%	8.932	9.097	9.995	10.333	10.665	11.519	12.212
VaR 95%	12.353	12.285	13.594	13.857	14.157	16.238	16.806
SSP370							
mean	4.879	6.618	5.866	6.703	6.979	7.617	8.432
median	3.556	3.885	4.339	4.736	5.147	5.611	6.136
VaR 90%	9.267	9.933	11.098	12.409	12.812	14.318	15.629
VaR 95%	12.186	13.360	15.114	16.174	17.576	19.176	21.410
SSP585							
mean	5.088	6.258	7.143	7.930	9.381	10.521	11.590
median	3.647	4.536	5.138	5.766	6.754	7.261	7.920
VaR 90%	9.487	11.747	13.650	14.957	17.362	18.580	20.547
VaR 95%	12.837	16.137	18.611	20.366	23.338	25.249	28.028

To examine the variability in estimates across GCMs, Figure 2 presents boxplots by decade for SSP245 and SSP585. Each boxplot represents the GCM variability - where each statistic (mean, VaR90%, VaR95%) is calculated only using the simulated losses for each GCM. The results demonstrate the projected increases across the decades and SSPs presented in Table 7. They also demonstrate higher levels of GCM uncertainty towards the end of the century. The VaR at 95% under SSP585 over the 2020s, has an inter-quartile range of 5.75 billion USD (15.35 billion USD (Q3) - 9.60 billion USD (Q1)) which increases to 13.33 billion USD in the 2080s. Comparing the variability between the SSPs (the two columns) and the GCMs (boxplots), it is evident that the GCM uncertainty dominates the future loss estimates, with the inter-quartile ranges greater than the median differences between SSPs. However, despite the large GCM variability, loss increases due to climate change are much worse under SSP585 than under SSP245. By the end of the century, SSP585 would double the VaR at 95%, whereas the percentage increase for SSP245 is in the order of 35% (compared to the 2020s). While the increases may be smaller than the inter-model variability, they still represent large increases in economic loss.

5 Discussion

Here we presented a methodology to project climate change risk that does not rely on heavily parameterized and computationally expensive CAT modeling. Our method also allows for examination of the uncertainty due to future climate projections and GCM choice. To the best of the authors' knowledge, this is the first study to link climate related economic losses directly to the hazard through non-stationary statistical modeling. While the methodology here is generic and could be applied to any hazard with corresponding economic loss data, we applied the methodology to flood losses and acknowledge several assumptions in our analysis.

Our analysis made no allowance for climate adaptation measures or changes in land cover, housing types or topography. It has been argued that adaptation measures may offset the increased frequency and magnitude of climatic events (Nicholls, 2011). How-

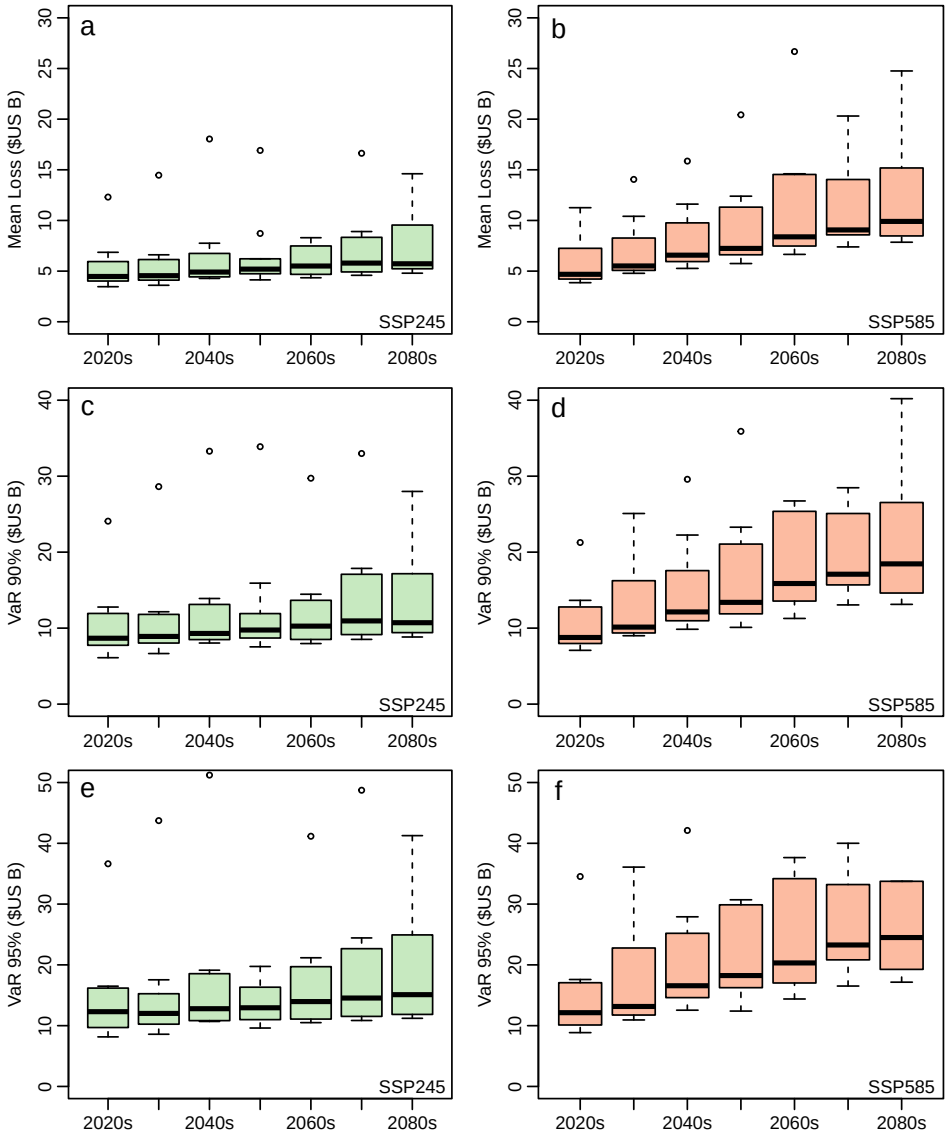

Figure 2. Projected Value at Risk. The left column (a, c, e) presents losses for SSP245, while the right column presents losses for SSP585 (b, d, f). The rows present the mean loss (a-b), VaR90% (c-d), and VaR95% (e-f)

ever it is noted that increased exposure of the climate events was modeled through an increase in the population density. Adaptation measures could be incorporated in the future through changes in the population density. We note it was assumed that projected population growth rates for the USA apply uniformly to all WNA states but this assumption could also be relaxed.

The SHELDUS database reports losses at the county level. However for many flood events, the total loss is equally allocated across the affected counties due to insufficient information. Indeed of the 6130 county level observations, 57% of losses were identical. Further, GCM grid sizes are larger than most counties. Given these limitations, we chose to model each WNA state as a single entity, that is a grid cell. We did not model tail-dependence across WNA states in the event severity, and only considered it for the event occurrence. This is due to the statistically insignificant levels of tail dependence in the per capita losses. If this work is to be repeated at a more spatially granular level, tail dependence could exist, requiring multivariate extreme value modeling. Future research could investigate the use of physically downscaled climate model simulations for higher spatial resolution loss projections, as well as extending the analysis to different regions and other types of extreme events.

Although per capita losses below the threshold (90th percentile) were assumed to be zero, it was also assumed that extreme floods occur when the values of the weather covariates are above their 90th percentile. To assess the reasonableness of this assumption, for each of the 146 historical extreme flood events, we calculated the percentile of precipitation driving the flood event, using the historical data for that state. The median precipitation percentile for the 146 events is 0.92, which suggests that this assumption is reasonable.

As per existing studies which model non-stationarity in flooding, the historical relationship between the covariates and extreme losses assumed time invariance. These relationships may be non-stationary, but testing this assumption is beyond the scope of this study. It may be surprising that temperature is never selected as a covariate. However, annual, or in this case, monthly local temperature, is a poor predictor of rainfall magnitude (Barbero et al., 2017) and by extension flood magnitude. Greater extreme events and flooding are generally associated with lower temperatures, due to the increase in the duration and frequency of rainfall events resulting in lower temperatures and a negative correlation (Wasko & Nathan, 2019b). This negative relation is inconsistent with the Clausius-Clapeyron equation, which will drive increased storm intensity and flooding over the coming century. Positive relationships only result if the temperature sampled is representative of the driving event (Visser et al., 2020, 2021). For completeness, the above analysis was repeated using the monthly temperature anomaly. The GPD results were similar to those obtained using temperature, i.e coefficient estimates were consistently negative and statistically insignificant.

The best performing conditional GPD models were more likely to have a non-stationary scale parameter (61 times) than shape parameter (15 times). This is consistent with (Davison & Smith, 1990) who suggest modeling the scale parameter conditionally, but the shape parameter unconditionally. While some studies (Jayaweera et al., 2025) suggest both the scale and shape parameter should be non-stationary, the additional uncertainty due to varying the shape parameter generally results in the simpler model being chosen based on statistical heuristics. The use of large scale GCM covariates for estimating flood risk is supported by the fact that large-scale climate variability can generally explain geographic differences in flood discharge (Kim et al., 2024). Indeed large scale GCM covariates similar to those used here, have previously been used to project the magnitude of future floods (Kim & Villarini, 2024).

Finally, we did not consider compound events, and only modeled pluvial flooding. Flooding in estuaries could occur due to a high sea level and high river flow (Zscheischler

et al., 2018, 2020). However, it is likely that due to the different meteorological drivers of coastal flooding a different set of covariates would need to be employed. The aim here was not to develop an all-encompassing model of future flood losses, but rather to demonstrate that future economic losses can be successfully modeled using extreme value analysis in a manner which is physically based. Risks associated with compound events as well as different hazards are left to future research.

6 Conclusions

Here we proposed a new approach to project future economic losses. The approach is general enough to be applied to any economic risk from extreme weather, and can incorporate both changes in the frequency of events as well as their severity. We employed a non-stationary multivariate Poisson distribution with a conditional non-stationary GPD, that linked the model parameters to climate and demographic covariates. Covariate projections from GCMs for SSPs 126, 245, 370 and 585 were then used to simulate aggregate losses. We illustrated the approach by estimating direct property damages from flooding across the Western North American states. Projections till the end of this century revealed that higher CO2 concentration levels reflected in the various SSPs significantly increase the potential losses from flooding, with estimates of losses using SSP585 twice the magnitude of those estimated under SSP126.

The good behaviour of our model on historical data suggests that the model estimates may reasonably approximate extreme property damage from floods in regions that have similar hydrological typology, weather systems and levels of economic development. This is important because loss data sets for other jurisdictions may not exist or lack the number of observations needed to reliably estimate conditional GPDs. Loss projections for similar regions, may therefore employ similar GPD parameter estimates to those used here with the relevant CMIP6 and demographic projections.

Avenues for further research include use of additional covariates that measure land use, hydrography, and the spatial distribution of population under various SSPs (Merkens et al., 2016). Future research could also consider other North American regions subject to hurricanes and compound events. As more granular geospatial loss data becomes available, our approach could also be used for smaller geographic regions with finer grid sizes and downscaled weather covariates. Finally, the method could also be applied to other disasters like droughts and fires.

Open Research Section

Loss data is obtained from the SHELDUS database https://cemhs.asu.edu/sheldus. Observed rainfall can be obtained https://doi.org/10.25914/5ca4c380b0d44 and observed temperature from https://www.ncei.noaa.gov/access/monitoring/climate-at-a-glance/statewide/time-series. GCM variables were calculated using climpact https://github.com/ARCCSS-extremes/climpact.

Acknowledgments

Conrad Wasko is supported by a University of Sydney Horizon Fellowship. Julia Neme is supported by ARC grant number CE170100023. Sarah Perkins-Kirkpatrick is supported by ARC grant number CE230100012.

References

Ackerman, F., DeCanio, S. J., Howarth, R. B., & Sheeran, K. (2009). Limitations of integrated assessment models of climate change. *Climatic change*, *95*, 297–315.

Alfieri, L., Feyen, L., Dottori, F., & Bianchi, A. (2015). Ensemble flood risk assessment in Europe under high end climate scenarios. *Global Environmental Change*, *35*, 199–212.

Arent, D. J., Tol, R. S., Faust, E., Hella, J. P., Kumar, S., Strzepek, K. M., ... Yan, D. (2014). Key economic sectors and services. In *Climate Change 2014: Impacts, Adaptation, and Vulnerability. Part A: Global and Sectoral Aspects. Contribution of Working Group II to the Fifth Assessment Report of the Intergovernmental Panel on Climate Change* (pp. 659–708). doi: 10.1017/CBO9781107415379.015

Arnell, N. W., & Gosling, S. N. (2016). The impacts of climate change on river flood risk at the global scale. *Climatic Change*, *134*, 387–401.

ASU Center for Emergency Management and Homeland Security. (2025). *The Spatial Hazard Events and Losses Database for the United States.* Phoenix, AZ: Arizona State University. Retrieved from `https://sheldus.org`

Barbero, R., Fowler, H. J., Lenderink, G., & Blenkinsop, S. (2017, January). Is the intensification of precipitation extremes with global warming better detected at hourly than daily resolutions? *Geophysical Research Letters*, *44*(2), 974–983. Retrieved from `http://doi.wiley.com/10.1002/2016GL071917` doi: 10.1002/2016GL071917

Beirlant, J., & Goegebeur, Y. (2003). Regression with response distributions of pareto-type. *Computational statistics & data analysis*, *42*(4), 595–619.

Bi, D., Dix, M., Marsland, S., O'farrell, S., Sullivan, A., Bodman, R., ... others (2020). Configuration and spin-up of ACCESS-CM2, the new generation Australian community climate and earth system simulator coupled model. *Journal of Southern Hemisphere Earth Systems Science*, *70*(1), 225–251.

Blöschl, G., Hall, J., Viglione, A., Perdigão, R. A. P., Parajka, J., Merz, B., ... Živković, N. (2019). Changing climate both increases and decreases European river floods. *Nature*, *573*(7772), 108–111. doi: 10.1038/s41586-019-1495-6

Bouwer, L. M. (2011, January). Have Disaster Losses Increased Due to Anthropogenic Climate Change? *Bulletin of the American Meteorological Society*, *92*(1), 39–46. Retrieved from `http://journals.ametsoc.org/doi/abs/10.1175/2011BAMS3167.1` (ISBN: 0003-0007) doi: 10.1175/2010BAMS3092.1

Bouwer, L. M., Bubeck, P., & Aerts, J. C. (2010). Changes in future flood risk due to climate and development in a Dutch polder area. *Global Environmental Change*, *20*(3), 463–471.

Burke, M., Davis, W. M., & Diffenbaugh, N. S. (2018). Large potential reduction in economic damages under UN mitigation targets. *Nature*, *557*(7706), 549–553.

Cabantous, L., & Dupont-Courtade, T. (2015). What is a Catastrophe Model Worth? *Making things valuable*, 167–186.

Changnon, S. A., Pielke Jr, R. A., Changnon, D., Sylves, R. T., & Pulwarty, R. (2000). Human factors explain the increased losses from weather and climate extremes. *Bulletin of the American Meteorological Society*, *81*(3), 437–442.

Contractor, S., Donat, M. G., Alexander, L. V., Ziese, M., Meyer-Christoffer, A., Schneider, U., ... Vose, R. S. (2020). Rainfall Estimates on a Gridded Network (REGEN)–a global land-based gridded dataset of daily precipitation from 1950 to 2016. *Hydrology and Earth System Sciences*, *24*(2), 919–943.

Crompton, R. P., & McAneney, K. J. (2008). Normalised Australian insured losses from meteorological hazards: 1967–2006. *Environmental Science & Policy*, *11*(5), 371–378.

Davison, A. C., & Smith, R. L. (1990). Models for exceedances over high thresholds. *Journal of the Royal Statistical Society: Series B (Methodological)*, *52*(3), 393–425.

Desmet, K., & Rossi-Hansberg, E. (2015). On the spatial economic impact of global warming. *Journal of Urban Economics*, *88*, 16–37.

Dottori, F., Szewczyk, W., Ciscar, J.-C., Zhao, F., Alfieri, L., Hirabayashi, Y., ...

Feyen, L. (2018, September). Increased human and economic losses from river flooding with anthropogenic warming. *Nature Climate Change*, *8*(9), 781–786. Retrieved 2025-05-18, from https://www.nature.com/articles/s41558-018-0257-z doi: 10.1038/s41558-018-0257-z

DuMouchel, W. H. (1983). Estimating the stable index *alpha* in order to measure tail thickness: A critique. *The Annals of Statistics*, *11*(4), 1019–1031.

Fadhel, S., Rico-Ramirez, M. A., & Han, D. (2018). Sensitivity of peak flow to the change of rainfall temporal pattern due to warmer climate. *Journal of Hydrology*, *560*, 546–559. Retrieved from https://doi.org/10.1016/j.jhydrol.2018.03.041 (Publisher: Elsevier B.V.) doi: 10.1016/j.jhydrol.2018.03.041

Fiedler, T., Wood, N., R Grose, M., & J Pitman, A. (2024, July). Storylines: A science-based method for assessing and measuring future physical climate-related financial risk. *Accounting & Finance*, acfi.13295. Retrieved 2024-09-10, from https://onlinelibrary.wiley.com/doi/10.1111/acfi.13295 doi: 10.1111/acfi.13295

Frame, D. J., Wehner, M. F., Noy, I., & Rosier, S. M. (2020). The economic costs of Hurricane Harvey attributable to climate change. *Climatic Change*, *160*(2), 271–281. (Publisher: Climatic Change) doi: 10.1007/s10584-020-02692-8

Goodess, C., Hanson, C., Hulme, M., & Osborn, T. (2003). Representing climate and extreme weather events in integrated assessment models: a review of existing methods and options for development. *Integrated Assessment*, *4*(3), 145–171.

Gründemann, G. J., van de Giesen, N., Brunner, L., & van der Ent, R. (2022). Rarest rainfall events will see the greatest relative increase in magnitude under future climate change. *Communications Earth and Environment*, *3*(235). (Publisher: Springer US ISBN: 4324702200558) doi: 10.1038/s43247-022-00558-8

Hakala, K., Addor, N., Teutschbein, C., Vis, M., Dakhlaoui, H., & Seibert, J. (2019). Hydrological Modeling of Climate Change Impacts. In *Encyclopedia of water: Science, technology, and society.* John Wiley & Sons, Inc. (Issue: February) doi: 10.1002/9781119300762.wsts0062

Held, H., Gerstengarbe, F. W., Pardowitz, T., Pinto, J. G., Ulbrich, U., Born, K., ... Burghoff, O. (2013). Projections of global warming-induced impacts on winter storm losses in the German private household sector. *Climatic Change*, *121*(2), 195–207. (ISBN: 0165-0009\r1573-1480) doi: 10.1007/s10584-013-0872-7

Hettiarachchi, S., Wasko, C., & Sharma, A. (2018, March). Increase in flood risk resulting from climate change in a developed urban watershed – the role of storm temporal patterns. *Hydrology and Earth System Sciences*, *22*(3), 2041–2056. Retrieved from https://doi.org/10.5194/hess-22-2041-2018 doi: 10.5194/hess-22-2041-2018

Hirabayashi, Y., Mahendran, R., Koirala, S., Konoshima, L., Yamazaki, D., Watanabe, S., ... Kanae, S. (2013, June). Global flood risk under climate change. *Nature Climate Change*, *3*(9), 816–821. Retrieved 2014-09-10, from http://www.nature.com/doifinder/10.1038/nclimate1911 (Publisher: Nature Publishing Group) doi: 10.1038/nclimate1911

Ho, M., O'Shea, D., Wasko, C., Nathan, R., & Sharma, A. (2025, January). *The impact of climate change on dam overtopping flood risk.* Engineering Hydrology/Stochastic approaches. Retrieved 2025-08-09, from https://hess.copernicus.org/preprints/hess-2024-403/ doi: 10.5194/hess-2024-403

Horowitz, J. K. (2009). The income–temperature relationship in a cross-section of countries and its implications for predicting the effects of global warming. *Environmental and Resource economics*, *44*(4), 475–493.

IPCC. (2012). *Managing the Risks of Extreme Events and Disasters to Ad-*

vance Climate Change Adaptation. A Special Report of Working Groups I and II of the Intergovernmental Panel on Climate Change. (C. B. Field et al., Eds.). Cambridge: Cambridge University Press. Retrieved from http://ebooks.cambridge.org/ref/id/CBO9781139177245 (arXiv: 1011.1669v3 ISSN: 16604601) doi: 10.1017/CBO9781139177245

Isphording, R. N., Alexander, L. V., Bador, M., Green, D., Evans, J. P., & Wales, S. (2024). A Standardized Benchmarking Framework to Assess Downscaled Precipitation Simulations. *Journal of Climate*, *37*(4), 1089–1110.

Iturbide, M., Gutiérrez, J. M., Alves, L. M., Bedia, J., Cerezo-Mota, R., Cimadevilla, E., ... Vera, C. S. (2020, November). An update of IPCC climate reference regions for subcontinental analysis of climate model data: definition and aggregated datasets. *Earth System Science Data*, *12*(4), 2959–2970. Retrieved 2025-08-09, from https://essd.copernicus.org/articles/12/2959/2020/ doi: 10.5194/essd-12-2959-2020

Ivancic, T. J., & Shaw, S. B. (2015, December). Examining why trends in very heavy precipitation should not be mistaken for trends in very high river discharge. *Climatic Change*, *133*(4), 681–693. Retrieved from http://link.springer.com/10.1007/s10584-015-1476-1 doi: 10.1007/s10584-015-1476-1

Jayaweera, L., Wasko, C., & Nathan, R. (2025, May). Evidence for Non-Stationarity in the GEV Shape Parameter When Modeling Extreme Rainfall. *Water Resources Research*, *61*(5), e2023WR036426. Retrieved 2025-05-05, from https://agupubs.onlinelibrary.wiley.com/doi/10.1029/2023WR036426 doi: 10.1029/2023WR036426

Jevrejeva, S., Jackson, L. P., Grinsted, A., Lincke, D., & Marzeion, B. (2018, July). Flood damage costs under the sea level rise with warming of 1.5 °C and 2 °C. *Environmental Research Letters*, *13*(7), 074014. Retrieved 2025-05-18, from https://iopscience.iop.org/article/10.1088/1748-9326/aacc76 doi: 10.1088/1748-9326/aacc76

Jongman, B., Kreibich, H., Apel, H., Barredo, J., Bates, P. D., Feyen, L., ... Ward, P. J. (2012). Comparative flood damage model assessment: towards a European approach. *Natural Hazards and Earth System Sciences*, *12*(12), 3733–3752.

Kahn, M. E., Mohaddes, K., Ng, R. N., Pesaran, M. H., Raissi, M., & Yang, J.-C. (2021). Long-term macroeconomic effects of climate change: A cross-country analysis. *Energy Economics*, *104*, 105624.

Khaliq, M., & Cunnane, C. (1996). Modelling point rainfall occurrences with the modified bartlett-lewis rectangular pulses model. *Journal of Hydrology*, *180*(1-4), 109–138.

Kharin, V. V., Zwiers, F. W., Zhang, X., & Hegerl, G. C. (2007, April). Changes in Temperature and Precipitation Extremes in the IPCC Ensemble of Global Coupled Model Simulations. *Journal of Climate*, *20*(8), 1419–1444. Retrieved 2013-08-16, from http://journals.ametsoc.org/doi/abs/10.1175/JCLI4066.1 doi: 10.1175/JCLI4066.1

Kim, H., & Villarini, G. (2024, January). Higher emissions scenarios lead to more extreme flooding in the United States. *Nature Communications*, *15*(1), 237. Retrieved 2025-05-19, from https://www.nature.com/articles/s41467-023-44415-4 doi: 10.1038/s41467-023-44415-4

Kim, H., Villarini, G., Wasko, C., & Tramblay, Y. (2024). Changes in the Climate System Dominate Inter-Annual Variability in Flooding Across the Globe. *Geophysical Research Letters*, *51*(6), e2023GL107480. doi: 10.1029/2023GL107480

Kundzewicz, Z. W., Kanae, S., Seneviratne, S. I., Handmer, J., Nicholls, N., Peduzzi, P., ... others (2014). Flood risk and climate change: global and regional perspectives. *Hydrological Sciences Journal*, *59*(1), 1–28.

Kupiec, P. (1995). *Techniques for verifying the accuracy of risk measurement models* (Vol. 95) (No. 24). Division of Research and Statistics, Division of Monetary Affairs, Federal Reserve Board.

Li, C., Zwiers, F., Zhang, X., Li, G., Sun, Y., & Wehner, M. (2021). Changes in annual extremes of daily temperature and precipitation in CMIP6 models. *Journal of Climate*, *34*(9), 3441–3460.

Lovato, T., Peano, D., Butenschön, M., Materia, S., Iovino, D., Scoccimarro, E., ... others (2022). CMIP6 simulations with the CMCC Earth system model (CMCC-ESM2). *Journal of Advances in Modeling Earth Systems*, *14*(3), e2021MS002814.

Ma, Y., Wei, B., & Huang, W. (2020). A nonparametric estimator for the conditional tail index of pareto-type distributions. *Metrika*, *83*, 17–44.

Madsen, H., Lawrence, D., Lang, M., Martinkova, M., & Kjeldsen, T. R. (2014). Review of trend analysis and climate change projections of extreme precipitation and floods in Europe. *Journal of Hydrology*, *519*(PD), 3634–3650. Retrieved from `http://dx.doi.org/10.1016/j.jhydrol.2014.11.003` (Publisher: Elsevier B.V.) doi: 10.1016/j.jhydrol.2014.11.003

Maposa, D., Cochran, J. J., et al. (2017). Modelling extreme flood heights in the lower Limpopo River basin of Mozambique using a time-heterogeneous generalised Pareto distribution. *Statistics and its Interface*, *10*(1), 131–144.

Mauritsen, T., Bader, J., Becker, T., Behrens, J., Bittner, M., Brokopf, R., ... others (2019). Developments in the MPI-M Earth System Model version 1.2 (MPI-ESM1. 2) and its response to increasing CO2. *Journal of Advances in Modeling Earth Systems*, *11*(4), 998–1038.

McDermott, T. K. (2022). Global exposure to flood risk and poverty. *Nature Communications*, *13*(1), 3529.

McNeil, A. J., & Frey, R. (2000). Estimation of tail-related risk measures for heteroscedastic financial time series: an extreme value approach. *Journal of empirical finance*, *7*(3-4), 271–300.

Merkens, J.-L., Reimann, L., Hinkel, J., & Vafeidis, A. T. (2016). Gridded population projections for the coastal zone under the shared socioeconomic pathways. *Global and Planetary Change*, *145*, 57–66.

Merz, B., Kreibich, H., Schwarze, R., & Thieken, A. (2010). Review article" assessment of economic flood damage". *Natural Hazards and Earth System Sciences*, *10*(8), 1697–1724.

Miller, J. D., & Hutchins, M. (2017). The impacts of urbanisation and climate change on urban flooding and urban water quality: A review of the evidence concerning the United Kingdom. *Journal of Hydrology: Regional Studies*, *12*(January), 345–362. Retrieved from `https://doi.org/10.1016/j.ejrh.2017.06.006` (Publisher: Elsevier) doi: 10.1016/j.ejrh.2017.06.006

Moscone, F., & Tosetti, E. (2009). A review and comparison of tests of cross-section independence in panels. *Journal of Economic Surveys*, *23*(3), 528–561.

Myhre, G., Alterskjær, K., Stjern, C. W., Hodnebrog, , Marelle, L., Samset, B. H., ... Stohl, A. (2019, December). Frequency of extreme precipitation increases extensively with event rareness under global warming. *Scientific Reports*, *9*, 16063. Retrieved from `http://www.nature.com/articles/s41598-019-52277-4` doi: 10.1038/s41598-019-52277-4

Neumayer, E., & Barthel, F. (2011). Normalizing economic loss from natural disasters: A global analysis. *Global Environmental Change*, *21*(1), 13–24. Retrieved from `http://dx.doi.org/10.1016/j.gloenvcha.2010.10.004` (Publisher: Elsevier Ltd ISBN: 0959-3780) doi: 10.1016/j.gloenvcha.2010.10.004

Newell, R. G., Prest, B. C., & Sexton, S. E. (2021). The GDP-temperature relationship: implications for climate change damages. *Journal of Environmental Economics and Management*, *108*, 102445.

Nicholls, N. (2011, June). Comments on "Have disaster losses increased due to an-

763 thropogenic climate change?". *Bulletin of the American Meteorological Society*,
764 *92*(6), 791–791. Retrieved from http://journals.ametsoc.org/doi/abs/10
765 .1175/2011BAMS3228.1 doi: 10.1175/2011BAMS3167.1
766 Ogden, F. (2021). *Geohydrology: Hydrological modeling, in Elias, Scott and Alder-*
767 *ton, David (eds), Encyclopedia of geology, Second edition.* Academic Press.
768 O'Neill, B. C., Tebaldi, C., Van Vuuren, D. P., Eyring, V., Friedlingstein, P., Hurtt,
769 G., ... Sanderson, B. M. (2016, September). The Scenario Model Intercom-
770 parison Project (ScenarioMIP) for CMIP6. *Geoscientific Model Development*,
771 *9*(9), 3461–3482. Retrieved 2025-08-09, from https://gmd.copernicus.org/
772 articles/9/3461/2016/ doi: 10.5194/gmd-9-3461-2016
773 Osman, Y. Z., Fealy, R., & Sweeney, J. C. (2015). Modelling extreme tempera-
774 tures in Ireland under global warming using a hybrid peak–over–threshold
775 and generalised Pareto distribution approach. *International Journal of Global*
776 *Warming*, *7*(1), 21–47.
777 O'Shea, D., Nathan, R., Wasko, C., Ho, M., & Sharma, A. (2024, August). Eval-
778 uation of key flood risk drivers under climate change using a bottom-up ap-
779 proach. *Journal of Hydrology*, *640*, 131694. Retrieved 2024-09-10, from
780 https://linkinghub.elsevier.com/retrieve/pii/S0022169424010904
781 doi: 10.1016/j.jhydrol.2024.131694
782 O'Shea, D., Nathan, R., Wasko, C., & Sharma, A. (2024). Separating storm inten-
783 sity and arrival frequency in nonstationary rainfall frequency analysis. *Water*
784 *Resources Research*, *60*(11), e2023WR036165.
785 Papalexiou, S. M., & Montanari, A. (2019). Global and Regional Increase of Pre-
786 cipitation Extremes Under Global Warming. *Water Resources Research*, 4901–
787 4914. doi: 10.1029/2018WR024067
788 Pezzey, J. C. (2019). Why the social cost of carbon will always be disputed. *Wiley*
789 *Interdisciplinary Reviews: Climate Change*, *10*(1), e558.
790 Rogers, J. S., Maneta, M. P., Sain, S. R., Madaus, L. E., & Hacker, J. P. (2025,
791 February). The role of climate and population change in global flood exposure
792 and vulnerability. *Nature Communications*, *16*(1), 1287. Retrieved 2025-08-
793 09, from https://www.nature.com/articles/s41467-025-56654-8 doi:
794 10.1038/s41467-025-56654-8
795 Scarrott, C., & MacDonald, A. (2012). A review of extreme value threshold estima-
796 tion and uncertainty quantification. *REVSTAT-Statistical journal*, *10*(1), 33–
797 60.
798 Seland, Ø., Bentsen, M., Olivié, D., Toniazzo, T., Gjermundsen, A., Graff, L. S., ...
799 others (2020). Overview of the Norwegian Earth System Model (NorESM2)
800 and key climate response of CMIP6 DECK, historical, and scenario simula-
801 tions. *Geoscientific Model Development*, *13*(12), 6165–6200.
802 Seneviratne, S., Nicholls, N., Easterling, D., Goodess, C., Kanae, S., Kossin, J., ...
803 Zhang, X. (2012). Changes in climate extremes and their impacts on the
804 natural physical environment. In C. B. Field et al. (Eds.), *Managing the Risk*
805 *of Extreme Events and Disasters to Advance Climate Change Adaptation* (pp.
806 109–230). A Special Report of Working Groups I and II of the Intergovern-
807 mental Panel on Climate Change (IPCC). Cambridge, UK, and New York,
808 NY, USA: Cambridge University Press.
809 Sharma, A., Wasko, C., & Lettenmaier, D. P. (2018, November). If Precipita-
810 tion Extremes Are Increasing, Why Aren't Floods? *Water Resources Re-*
811 *search*, *54*(11), 8545–8551. Retrieved from http://doi.wiley.com/10.1029/
812 2018WR023749 doi: 10.1029/2018WR023749
813 Sun, Q., Zhang, X., Zwiers, F., Westra, S., & Alexander, L. V. (2021, January). A
814 Global, Continental, and Regional Analysis of Changes in Extreme Precipita-
815 tion. *Journal of Climate*, *34*(1), 243–258. Retrieved from https://doi.org/
816 10.1175/JCLI-D-19-0892.1 doi: 10.1175/JCLI-D-19-0892.1
817 Swart, N. C., Cole, J. N., Kharin, V. V., Lazare, M., Scinocca, J. F., Gillett, N. P.,

... others (2019). The Canadian earth system model version 5 (CanESM5. 0.3). *Geoscientific Model Development*, *12*(11), 4823–4873.

Tatebe, H., Ogura, T., Nitta, T., Komuro, Y., Ogochi, K., Takemura, T., ... others (2019). Description and basic evaluation of simulated mean state, internal variability, and climate sensitivity in MIROC6. *Geoscientific Model Development*, *12*(7), 2727–2765.

Thistlethwaite, J., Minano, A., Blake, J. A., Henstra, D., & Scott, D. (2018). Application of re/insurance models to estimate increases in flood risk due to climate change. *Geoenvironmental Disasters*, *5*(1), 1–13.

Tol, R. S. (2002). Estimates of the damage costs of climate change. part 1: Benchmark estimates. *Environmental and resource Economics*, *21*(1), 47–73.

Tol, R. S. (2024). A meta-analysis of the total economic impact of climate change. *Energy Policy*, *185*, 113922.

Trenberth, K. E., Dai, A., Rasmussen, R. M., & Parsons, D. B. (2003, September). The changing character of precipitation. *Bulletin of the American Meteorological Society*, *84*(9), 1205–1217. Retrieved 2013-11-11, from `http://journals.ametsoc.org/doi/abs/10.1175/BAMS-84-9-1205` doi: 10.1175/BAMS-84-9-1205

Villarini, G., & Wasko, C. (2021, September). Humans, climate and streamflow. *Nature Climate Change*, *11*(9), 725–726. Retrieved from `https://doi.org/10.1038/s41558-021-01137-z` (Publisher: Springer US ISBN: 4155802101137) doi: 10.1038/s41558-021-01137-z

Visser, J. B., Wasko, C., Sharma, A., & Nathan, R. (2020, September). Resolving Inconsistencies in Extreme Precipitation-Temperature Sensitivities. *Geophysical Research Letters*, *47*(18), e2020GL089723. Retrieved from `https://doi.org/10.1029/2020GL089723` doi: 10.1029/2020GL089723

Visser, J. B., Wasko, C., Sharma, A., & Nathan, R. (2021, September). Eliminating the "hook" in Precipitation-Temperature Scaling. *Journal of Climate*, *34*(23), 9535–9549. Retrieved from `https://journals.ametsoc.org/view/journals/clim/aop/JCLI-D-21-0292.1/JCLI-D-21-0292.1.xml` doi: 10.1175/JCLI-D-21-0292.1

Wang, X., Hyndman, R. J., Li, F., & Kang, Y. (2023). Forecast combinations: An over 50-year review. *International Journal of Forecasting*, *39*(4), 1518–1547.

Wasko, C. (2022, December). Floods differ in a warmer future. *Nature Climate Change*, *12*(12), 1090–1091. Retrieved from `https://www.nature.com/articles/s41558-022-01541-z` (Publisher: Springer US ISBN: 4155802201) doi: 10.1038/s41558-022-01541-z

Wasko, C., Guo, D., Ho, M., Nathan, R., & Vogel, E. (2023). Diverging projections for flood and rainfall frequency curves. *Journal of Hydrology*, *620*(October 2022), 129403. doi: 10.1016/j.jhydrol.2023.129403

Wasko, C., & Nathan, R. (2019a, August). Influence of changes in rainfall and soil moisture on trends in flooding. *Journal of Hydrology*, *575*(November 2018), 432–441. Retrieved from `https://linkinghub.elsevier.com/retrieve/pii/S0022169419304998` (Publisher: Elsevier) doi: 10.1016/j.jhydrol.2019.05.054

Wasko, C., & Nathan, R. (2019b, September). The local dependency of precipitation on historical changes in temperature. *Climatic Change*, *156*(1-2), 105–120. Retrieved from `http://link.springer.com/10.1007/s10584-019-02523-5` (Publisher: Climatic Change) doi: 10.1007/s10584-019-02523-5

Weinkle, J., & Pielke Jr, R. (2017). The truthiness about hurricane catastrophe models. *Science, Technology, & Human Values*, *42*(4), 547–576.

Weitzman, M. L. (2009). On modeling and interpreting the economics of catastrophic climate change. *The review of economics and statistics*, *91*(1), 1–19.

Westra, S., Fowler, H., Evans, J., Alexander, L., Berg, P., Johnson, F., ... Roberts, N. (2014, July). Future changes to the intensity and frequency of short-duration extreme rainfall. *Reviews of Geophysics*, *52*(3), 522–555. Re-

trieved 2014-07-27, from http://onlinelibrary.wiley.com/doi/10.1029/88EO01108/abstract doi: 10.1002/2014RG000464

Wu, T., Lu, Y., Fang, Y., Xin, X., Li, L., Li, W., ... others (2019). The Beijing Climate Center climate system model (BCC-CSM): The main progress from CMIP5 to CMIP6. *Geoscientific Model Development*, *12*(4), 1573–1600.

Yahav, I., & Shmueli, G. (2012). On generating multivariate poisson data in management science applications. *Applied Stochastic Models in Business and Industry*, *28*(1), 91–102.

Yang, Y., Roderick, M. L., Yang, D., Wang, Z., Ruan, F., McVicar, T. R., ... Beck, H. E. (2021). Streamflow stationarity in a changing world. *Environmental Research Letters*, *16*(6), 064096. doi: 10.1088/1748-9326/ac08c1

Zhang, S., Zhou, L., Zhang, L., Yang, Y., Wei, Z., Zhou, S., ... Dai, Y. (2022, December). Reconciling disagreement on global river flood changes in a warming climate. *Nature Climate Change*, *12*(12), 1160–1167. Retrieved from https://www.nature.com/articles/s41558-022-01539-7 doi: 10.1038/s41558-022-01539-7

Ziehn, T., Chamberlain, M. A., Law, R. M., Lenton, A., Bodman, R. W., Dix, M., ... Srbinovsky, J. (2020). The Australian earth system model: ACCESS-ESM1. 5. *Journal of Southern Hemisphere Earth Systems Science*, *70*(1), 193–214.

Zscheischler, J., Martius, O., Westra, S., Bevacqua, E., Raymond, C., Horton, R. M., ... Vignotto, E. (2020, June). A typology of compound weather and climate events. *Nature Reviews Earth & Environment*, *1*(7), 333–347. Retrieved 2025-08-09, from https://www.nature.com/articles/s43017-020-0060-z doi: 10.1038/s43017-020-0060-z

Zscheischler, J., Westra, S., Van Den Hurk, B. J., Seneviratne, S. I., Ward, P. J., Pitman, A., ... Zhang, X. (2018). Future climate risk from compound events. *Nature Climate Change*, *8*(6), 469–477. Retrieved from http://dx.doi.org/10.1038/s41558-018-0156-3 (Publisher: Springer US) doi: 10.1038/s41558-018-0156-3

fbe.unimelb.edu.au/finance